Oxidation of isobutane over Mo–V–Sb mixed oxide catalyst

Tetsuya Shishido *, Atsushi Inoue, Tsuyoshi Konishi, Ikuya Matsuura and Katsuomi Takehira *

Department of Applied Chemistry, Faculty of Engineering, Hiroshima University, Kagamiyama 1-4-1, Higashi-hiroshima, Hiroshima 739-8527, Japan

E-mail: shishido@hiroshima-u.ac.jp

Received 22 February 2000; accepted 27 June 2000

The catalytic performances of Mo–V–Sb mixed oxide catalysts have been studied in the selective oxidation of isobutane into methacrolein. V–Sb mixed oxide showed the activity for oxidative dehydrogenation of isobutane to isobutene. The selectivity to methacrolein increased by the addition of molybdenum species to the V–Sb mixed oxide catalyst. In a series of Mo–V–Sb oxide catalysts, $Mo_1V_1Sb_{10}O_x$ exhibited the highest selectivity to methacrolein at 440 °C. The structure analyses by XRD, laser Raman spectroscopy and XPS showed the coexistence of highly dispersed molybdenum suboxide, $VSbO_4$ and α-Sb_2O_4 phases in the $Mo_1V_1Sb_{10}O_x$. The high catalytic activity of $Mo_1V_1Sb_{10}O_x$ can be explained by the bifunctional mechanism of highly dispersed molybdenum suboxide and $VSbO_4$ phases. It is likely that the oxidative dehydrogenation of isobutane proceeds on the $VSbO_4$ phase followed by the oxidation of isobutene into methacrolein on the molybdenum suboxide phase.

Keywords: Mo–V–Sb mixed oxide catalyst, selective oxidation, isobutane, methacrolein, XRD, Raman spectroscopy, XPS

1. Introduction

Selective conversion of alkanes to the oxygenated products by gaseous oxygen is an important process in the chemical industry [1–4]. However, the selective oxidation of light alkanes is usually accompanied by many difficulties as a result of the high reactivity of the oxygenated products compared to the low reactivity of alkanes under the reaction conditions. Because of the inertness of alkanes, reaction conditions are normally more severe than in the case of alkene oxidation, so that the subsequent oxidation of the partially oxidized products is unavoidable, resulting in low selectivity to the desired products. Since liquefied petroleum gas (LPG) is abundant and contains mainly propane and butanes, the selective conversions of these alkanes received attention. Among butanes, n-butane can be selectively oxidized to maleic anhydride by using crystalline V–P–O catalysts [5].

Recently, many patents have been disclosed for the partial oxidation of propane, among which the ammoxidation to acrylonitrile is the most prominent [6,7]. Several catalytic systems based on mixed oxide have been tested [6–10], but only a few showed good catalytic performances. The V–Sb mixed oxide based catalysts seem to be selective for producing acrylonitrile [9,11–15]. It is likely that vanadium-based compounds have an important role in the alkane activation not only in ammoxidation but also in partial oxidation by gaseous oxygen. In fact, many kinds of vanadium-based mixed oxide catalysts have been investigated [1–15]. Also, it is well known that molybdenum-based mixed oxides are one of the key components for alkene oxidation to oxygenated compounds [16].

In the present study, we report the promotion effect of molybdenum species on V–Sb mixed oxide catalysts for the oxidation of isobutane. We prepared the Mo–V–Sb mixed oxide catalysts and investigated the catalytic behavior for oxidation of isobutane by gaseous oxygen as well as the structure analyses by XRD, Raman spectroscopy and XPS. The catalytic activity was discussed in relation to the structure and the surface acidic property characterized by NH_3-TPD.

2. Experimental

2.1. Catalyst preparation

Mo–V–Sb mixed oxide catalysts were prepared by the following slurry method. Sb_2O_3 (Wako Pure Chemical Industries) was dispersed in oxalic acid aqueous solution, in which a hot aqueous solution of NH_4VO_3 and $(NH_4)_3Mo_7O_{24}{\cdot}4H_2O$ (Wako Pure Chemical Industries) was added. The atomic ratios of V/Sb and Mo/Sb were changed between 0.1–2.0 and 0.01–1.0, respectively. The mixture was heated under reflux conditions at 90 °C for 24 h. The precipitate was separated from the solution by evaporating at 80 °C. The resulting mixture was dried at 100 °C for 15 h, followed by grinding into a fine powder, calcination at 350 °C for 4 h and finally at 600 °C for 6 h in air. A similar procedure was also applied in the preparation of V–Sb or Mo–Sb mixed oxide catalysts. Sb_2O_3, MoO_3 and V_2O_5 were purchased (Wako Pure Chemical Industries) and used without further purification. α-Sb_2O_4 was prepared by calcination of Sb_2O_3 at 600 °C for 6 h in air.

* To whom correspondence should be addressed.

2.2. Characterization of catalysts

Metal compositions of the catalysts were calculated based on the amount of starting compounds in the preparation. Surface areas of the catalysts were measured from the adsorption isotherms of N_2 at 77 K using the BET method (BEL Japan BELSORP18SP). X-ray diffraction measurements were performed on a Rigaku RINT2500VHF using Cu Kα radiation. Laser Raman spectra were taken with the 514.5 nm line of the argon laser (JASCO NRS-2100) at room temperature. The incident laser power at the samples was 20 mW, and spectra were recorded with a resolution of 4 cm^{-1}. XPS measurements were recorded on a VG ESCALAB220I-XL system with monochromatic Al Kα (1486.6 eV) as the X-ray source. The C 1s as a reference signal was adjusted to 284.6 eV. TPD (temperature-programmed desorption) of adsorbed NH_3 was performed on a BEL Japan TPD-1-AT in order to evaluate the catalyst surface acidity. The structures of both $V_1Sb_{10}O_x$ and $Mo_1V_1Sb_{10}O_x$ after the reaction were also studied by XRD, Raman, and XPS.

2.3. Catalytic reactions

The oxidation of isobutane with gaseous oxygen was carried out using a conventional flow system equipped with a U-shaped Pyrex tube reactor at the temperature of 440–560 °C under atmospheric pressure. The catalyst (2.0 g) was diluted with 1.0 g of quartz grains. The feed gas consisted of 50 vol% of isobutane, 16.7 vol% O_2 and N_2 balance. Total flow rate was 40 $cm^3\,min^{-1}$ (GHSV = 900 $ml\,h^{-1}\,g\text{-}cat^{-1}$). The ammoxidation of propane was also carried out using the catalyst (1.5 g) diluted with 1.0 g of quartz grains. The feed gas consisted of 15 vol% of propane, 30 vol% of O_2, 15 vol% of NH_3 and N_2 balance. Total flow rate was 40 $cm^3\,min^{-1}$ (GHSV = 1600 $ml\,h^{-1}\,g\text{-}cat^{-1}$). Prior to the reaction, the catalyst was treated at 500 °C in 25 vol% of O_2 in N_2 stream (GHSV = 450 $ml\,h^{-1}\,g\text{-}cat^{-1}$) for 2 h, and then cooled down to the reaction temperature under the same atmosphere. The feedstock and products were analyzed by on-line FID and TCD gas chromatographs.

3. Results and discussion

3.1. Characterization of the V–Sb and Mo–V–Sb mixed oxide catalysts

3.1.1. XRD measurements

Figure 1 shows XRD patterns of V–Sb mixed oxide catalysts with the various V/Sb atomic ratios. Surface areas of the catalysts and phases identified by XRD are summarized in table 1. In the XRD patterns of both $V_2Sb_1O_x$ and $V_1Sb_1O_x$, three phases ($VSbO_4$, α-Sb_2O_4 and V_2O_5) were observed. The diffraction peaks of the V_2O_5 phase could not be observed in the V–Sb mixed oxide catalysts containing vanadium below the atomic ratio of V/Sb = 1.0,

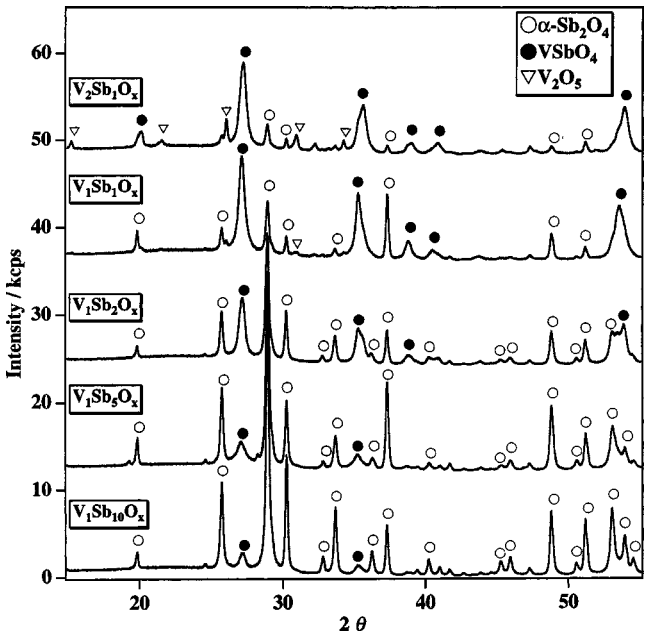

Figure 1. X-ray diffraction patterns of the V–Sb mixed oxide catalysts.

Table 1
BET surface areas of the catalysts.

Catalyst[a]	Surface area[b] ($m^2\,g^{-1}$)	Phase observed
$V_2Sb_1O_x$	13.7	$VSbO_4$, α-Sb_2O_4, V_2O_5
$V_1Sb_1O_x$	17.8	$VSbO_4$, α-Sb_2O_4, V_2O_5
$V_1Sb_2O_x$	6.0	$VSbO_4$, α-Sb_2O_4
$V_1Sb_5O_x$	7.5	$VSbO_4$, α-Sb_2O_4
$V_1Sb_{10}O_x$	10.7	$VSbO_4$, α-Sb_2O_4
$Mo_{0.1}V_1Sb_{10}O_x$	10.2	$VSbO_4$, α-Sb_2O_4
$Mo_{0.5}V_1Sb_{10}O_x$	10.0	$VSbO_4$, α-Sb_2O_4
$Mo_1V_1Sb_{10}O_x$	8.2	$VSbO_4$, α-Sb_2O_4
$Mo_5V_1Sb_{10}O_x$	8.7	MoO_3, $VSbO_4$, α-Sb_2O_4
$Mo_{10}V_1Sb_{10}O_x$	16.6	MoO_3, $VSbO_4$, α-Sb_2O_4
$Mo_1Sb_{10}O_x$	5.4	α-Sb_2O_4
V_2O_5	5.1	V_2O_5
MoO_3	3.4	MoO_3
α-Sb_2O_4	3.2	α-Sb_2O_4

[a] Atomic ratio calculated from the amount of reagents.
[b] BET surface area, N_2 at 77 K.

indicating that crystalline V_2O_5 is absent in these catalysts. The intensities of the $VSbO_4$ rutile phase increased, while the intensities of the α-Sb_2O_4 phase decreased, with increasing the V/Sb ratio. The V–Sb mixed oxide catalysts consist of both $VSbO_4$ and α-Sb_2O_4 phases up to the ratio of V/Sb = 1.0, while the V_2O_5 phase appeared when the V/Sb ratio exceeded 1.0.

Figure 2 shows XRD patterns of Mo–V–Sb mixed oxide catalysts with the various Mo/Sb atomic ratios. The V/Sb ratio was fixed at 0.1. In the Mo–V–Sb mixed oxide catalysts, $VSbO_4$ and α-Sb_2O_4 were again observed. When the Mo/Sb ratio was increased, the MoO_3 phase appeared and increased its intensity, suggesting that MoO_3 is isolated even at low content of Mo and its crystalline size increases with the content. In the case of $Mo_{10}V_1Sb_{10}O_x$ catalyst,

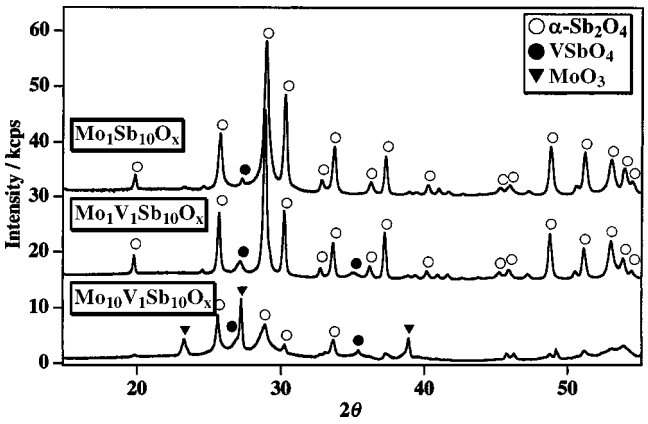

Figure 2. X-ray diffraction patterns of the $Mo_{10}V_1Sb_{10}O_x$, $Mo_1V_1Sb_{10}O_x$ and $Mo_1Sb_{10}O_x$ catalysts.

three intense diffraction peaks of MoO_3 were observed at $2\theta = 23.3°$, 27.2° and 38.9°. In the XRD pattern of the Mo–V–Sb mixed oxide catalyst with molybdenum below the ratio of Mo/Sb = 0.2, no peak due to MoO_3 was observed. The XRD pattern of $Mo_1V_1Sb_{10}O_x$ showed no substantial change even after the catalytic reaction at 520 °C except that the intensities of the $VSbO_4$ rutile phase slightly decreased. In the case of $Mo_1Sb_{10}O_x$ (without vanadium ions), intense diffraction peaks due to the α-Sb_2O_4 phase were observed together with weak peaks due to the MoO_3 phase. In spite of the presence of both molybdenum and antimony species, the diffraction peaks of Mo–Sb mixed oxides (for example, Sb_2MoO_6 (JCPDS 33-1491), $Sb_2Mo_{10}O_{31}$ (JCPDS 33–0105) and $Sb_4Mo_{10}O_{31}$ (JCPDS 33-0104)) could not be observed in all the Mo–V–Sb mixed oxide catalysts prepared.

3.1.2. Laser Raman spectra

Raman spectra of $V_1Sb_{10}O_x$, $Mo_1V_1Sb_{10}O_x$ and $Mo_{10}V_1Sb_{10}O_x$ catalysts and metal oxides (V_2O_5, MoO_3 and α-Sb_2O_4) were recorded at room temperature, and are shown in figures 3 and 4, respectively. In the spectrum of $V_1Sb_{10}O_x$, four bands at 460, 401, 263 and 198 cm^{-1} were observed and can be assigned to α-Sb_2O_4, suggesting that the surface of $V_1Sb_{10}O_x$ is partly covered by α-Sb_2O_4. Crystalline V_2O_5 exhibits bands at 996, 702, 529, 482, 407, 305 and 285 cm^{-1} [17–19], which, however, could not be observed, indicating that crystalline V_2O_5 is absent on this catalyst. This result is consistent with that obtained by XRD. Monomeric species such as $(V{=}O)O_3$ on silica [18,19] and tetrahedrally coordinated vanadium species on silica [20] show a band at 1020–1040 cm^{-1}. In the spectrum of $V_1Sb_{10}O_x$, the band at 1020–1040 cm^{-1} could not be detected even at the ratio of V/Sb = 0.1, suggesting that vanadium species in $V_1Sb_{10}O_x$ are not isolated as the monomeric one.

In the spectrum of $Mo_{10}V_1Sb_{10}O_x$, neither the bands of α-Sb_2O_4 nor the bands of crystalline V_2O_5 phases could be observed, but four strong bands appeared at 996, 820, 666 and 380 cm^{-1}. These bands can be assigned to crystalline MoO_3 [21,22]. Indeed, in the spectrum of crystalline MoO_3 in figure 4, bands at 996, 819, 667, 378, 366 and 284 cm^{-1} were observed. These results indicate that the most part of molybdenum ions form crystalline MoO_3 on the surface of $Mo_{10}V_1Sb_{10}O_x$. In contrast, in the spectrum of $Mo_1V_1Sb_{10}O_x$, neither MoO_3 nor V_2O_5 phase was observed, but seven bands appeared at 860(s), 810(sh), 492(m), 454(m), 399(m), 266(w) and 198(m) cm^{-1}. The four bands at 454(m), 399(m), 266(w) and 198(m) cm^{-1} can be assigned to α-Sb_2O_4 (figure 4), indicating that the surface of $Mo_1V_1Sb_{10}O_x$ is partly covered by an α-Sb_2O_4 phase. Gaigneaux et al. [23] and Spevack et al. [24] reported that MoO_2 shows seven weak bands at 741, 568,

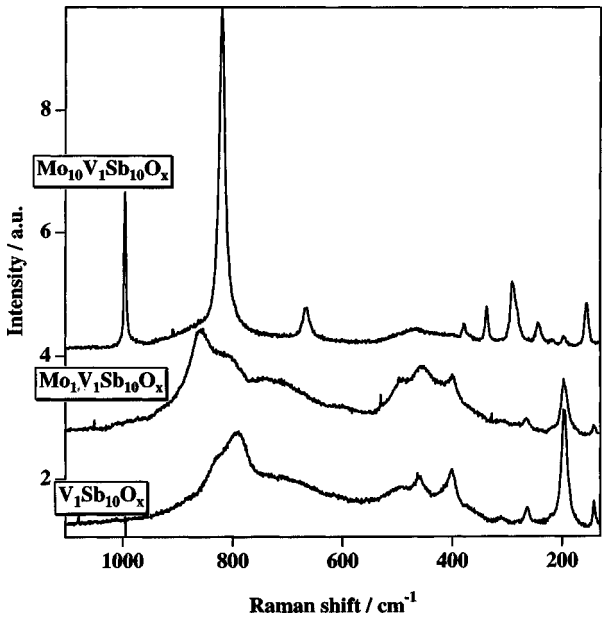

Figure 3. Raman spectra of the $V_1Sb_{10}O_x$, $Mo_1V_1Sb_{10}O_x$ and $Mo_{10}V_1Sb_{10}O_x$ catalysts.

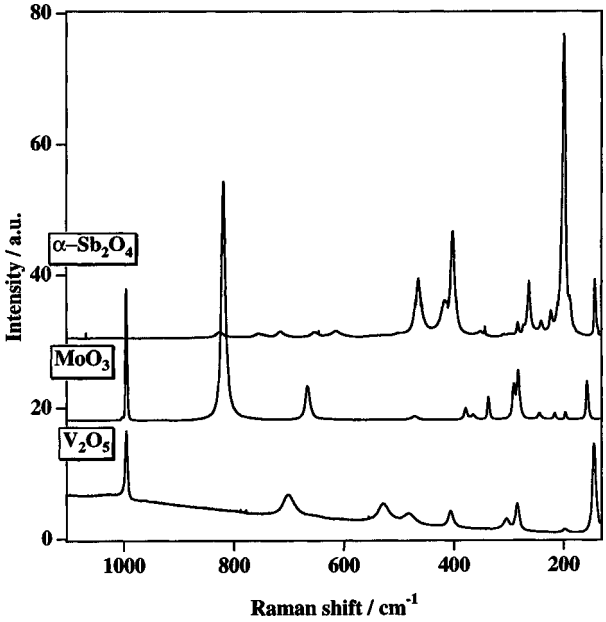

Figure 4. Raman spectra of V_2O_5, MoO_3 and α-Sb_2O_4.

495, 466, 362, 227 and 202 cm^{-1}. The bands found in the spectrum of $Mo_1V_1Sb_{10}O_x$ are not identical to those of the MoO_2. Mo–Sb mixed oxide can be formed in the present Mo–V–Sb mixed oxide catalyst. However, this possibility was clearly discarded, since none of three types of Mo–Sb mixed oxides (Sb_2MoO_6, $Sb_2Mo_{10}O_{31}$ and $Sb_4Mo_{10}O_{31}$) was detected in both $Mo_1V_1Sb_{10}O_x$ and $Mo_1Sb_{10}O_x$ by XRD. The bands actually found in the Raman spectrum of $Mo_1V_1Sb_{10}O_x$ are not consistent with any of Sb_2MoO_6 and $Sb_2Mo_{10}O_{31}$ reported by Gaigneaux et al. [23]. Pamentier et al. [25–27] reported that the Sb_2MoO_6 phase was found by calcination around 500 °C under low pressure of argon atmosphere, while $Sb_2Mo_{10}O_{31}$ or $Sb_4Mo_{10}O_{31}$ was formed by calcination around 500 °C under nitrogen atmosphere with a small amount of hydrogen and high concentration of water vapor. However, these Mo–Sb mixed oxides decompose to a mixture of MoO_3 and α-Sb_2O_4 in air between 350 and 400 °C. Gaigneaux et al. [23] also reported that the decomposition started between 300 and 400°C for both Sb_2MoO_6 and $Sb_2Mo_{10}O_{31}$ and between 400 and 500 °C for $Sb_4Mo_{10}O_{31}$ in air. In the present work, both $Mo_1V_1Sb_{10}O_x$ and $Mo_1Sb_{10}O_x$ were calcined at 600 °C, which is clearly higher than the decomposition temperature, in air. This might be the most plausible reason of the absence of the Mo–Sb mixed oxide phase.

In vibration modes due to the Mo–O–Mo bond in many molybdenum samples, the symmetric stretching, asymmetric stretching and deformation vibrations are observed at 450–650, 700–900 and 170–230 cm^{-1}, respectively [21]. Therefore, it is most likely that the bands at 860(s), 810(sh) and 495(sh) cm^{-1} are assignable to the Mo–O–Mo bond and, while the band at 198(m) cm^{-1} is to α-Sb_2O_4, in the spectrum of $Mo_1V_1Sb_{10}O_x$. The bands at 860(s), 810(sh) and 495(sh) are different from those of crystalline MoO_3 having octahedral coordination around molybdenum ions, suggesting that the molybdenum species has distorted octahedral coordination around molybdenum in the $Mo_1V_1Sb_{10}O_x$ catalyst.

After the catalytic reaction at 520 °C, the Raman spectrum of $Mo_1V_1Sb_{10}O_x$ slightly changed. The relative intensities of the bands at 452, 398, 264 and 198 cm^{-1}, which can be assigned to α-Sb_2O_4, increased and a new intense band at 818 cm^{-1} appeared, while the bands at 860(s), 810(sh) and 495(sh) cm^{-1} were still observed, indicating that the molybdenum species of distorted octahedral coordination still remained. The band at 818 cm^{-1} corresponds to that of the Mo–O–Mo bond in crystalline MoO_3, suggesting that a part of Mo species aggregated on the $Mo_1V_1Sb_{10}O_x$. In the XRD pattern of $Mo_1V_1Sb_{10}$ after the reaction, no XRD peaks due to MoO_3 were observed, indicating that the size of MoO_3 is quite small even after the reaction.

3.1.3. XPS measurement

The peak of the V $2p_{3/2}$ in $V_1Sb_{10}O_x$ is assigned to the V^{4+} state and shifted to low binding energy by the addition of Mo ions to $V_1Sb_{10}O_x$, indicating that the electron densities on vanadium in the Mo–V–Sb mixed oxide increases compared to that in $V_1Sb_{10}O_x$. Even after 6 h of the reaction at 520 °C, the V $2p_{3/2}$ peaks in both $V_1Sb_{10}O_x$ and $Mo_1V_1Sb_{10}O_x$ are still assigned to V^{4+} state. In both the $V_1Sb_{10}O_x$ and $Mo_1V_1Sb_{10}O_x$ catalysts, the surface atomic ratios V/Sb determined by XPS were much smaller than the values estimated from the starting composition. It is likely that a large excess of antimony was present on the surface of both V–Sb and Mo–V–Sb mixed oxide catalysts.

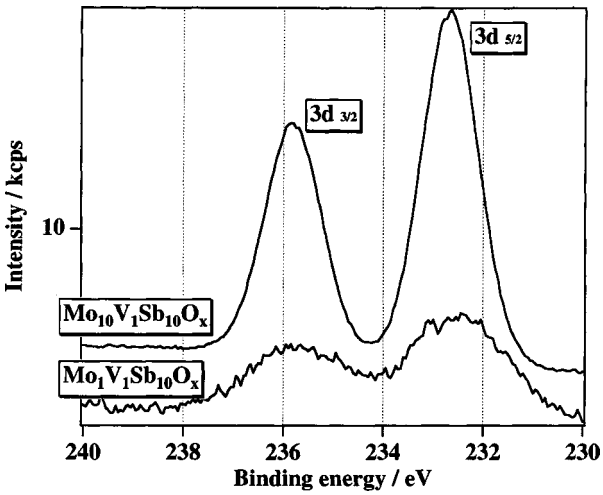

Figure 5. Mo 3d XPS spectra of the $Mo_1V_1Sb_{10}O_x$ and $Mo_{10}V_1Sb_{10}O_x$ catalysts.

The Mo 3d spectra of $Mo_1V_1Sb_{10}O_x$ and $Mo_{10}V_1Sb_{10}O_x$ are shown in figure 5. The intensities of the Mo 3d peaks of $Mo_{10}V_1Sb_{10}O_x$ are stronger than those of $Mo_1V_1Sb_{10}O_x$, suggesting that the surface concentration of Mo species is higher on the former than the latter. The binding energies of the Mo 3d peaks of $Mo_{10}V_1Sb_{10}O_x$ correspond to Mo^{6+}. Taking into account the XRD and Raman spectroscopy results, the most part of molybdenum species form MoO_3 in $Mo_{10}V_1Sb_{10}O_x$. On the other hand, the valence state of molybdenum in $Mo_1V_1Sb_{10}O_x$ is a mixture of Mo^{5+} and Mo^{6+} judging from the binding energies and peak widths of the Mo 3d peaks. It is likely that molybdenum oxide species in $Mo_1V_1Sb_{10}O_x$ were partly reduced to "suboxides", i.e., Mo_8O_{23}, Mo_9O_{26} or $Mo_{18}O_{52}$. However, any kind of these reduced species could not be detected by XRD. On the basis of these results, we propose a surface structure of the catalyst where the small suboxide particles (<40 Å) are highly dispersed on the surface of $Mo_1V_1Sb_{10}O_x$. Even after the catalytic reaction at 520 °C, the valence state of molybdenum in $Mo_1V_1Sb_{10}O_x$ can still be assigned to the mixture of Mo^{5+} and Mo^{6+}. This result suggests that small suboxide particles were present on the surface of $Mo_1V_1Sb_{10}O_x$ during the reaction.

3.1.4. TPD of adsorbed NH_3 measurements

To examine the acidic property of the $V_1Sb_{10}O_x$, $Mo_1V_1Sb_{10}O_x$ and $Mo_{10}V_1Sb_{10}O_x$ catalysts, NH_3-TPD was carried out and the profiles are shown in figure 6. On

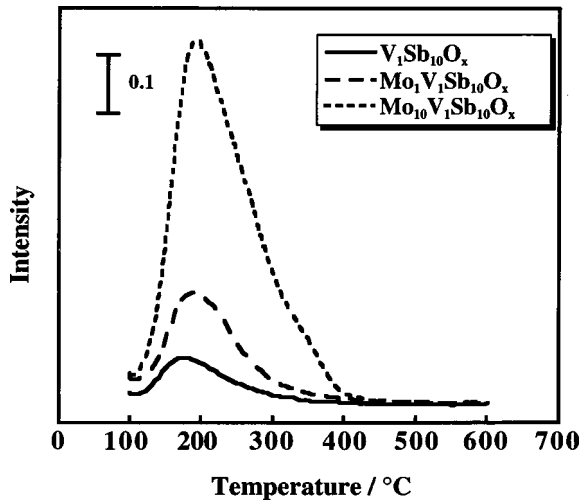

Figure 6. NH_3-TPD plots of the $V_1Sb_{10}O_x$, $Mo_1V_1Sb_{10}O_x$ and $Mo_{10}V_1Sb_{10}O_x$ catalysts.

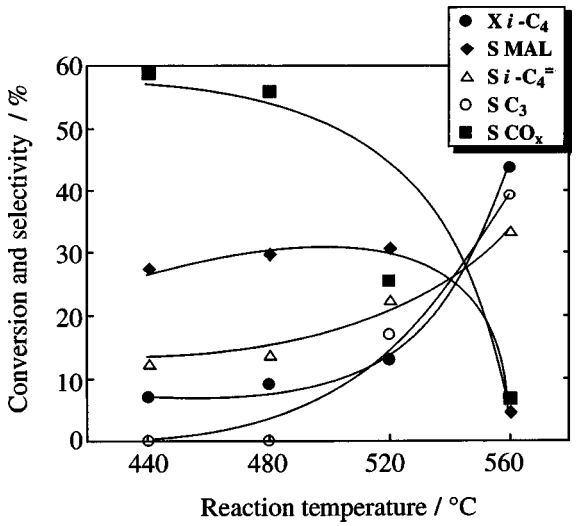

Figure 7. Isobutane oxidation over the $Mo_1V_1Sb_{10}O_x$ catalyst. i-C_4H_{10}/O_2/N_2 = 15/5/10 ($cm^3\,min^{-1}$); SV = 900 $cm^3\,h^{-1}\,g^{-1}$.

$V_1Sb_{10}O_x$, a small amount of NH_3 was desorbed with a peak temperature of 180 °C. On $Mo_1V_1Sb_{10}O_x$, the amount of desorbed NH_3 is about 2.5 times larger than that of $V_1Sb_{10}O_x$ and the peak temperature increased to 200 °C. Thus, the acidity on the catalysts increased by the addition of molybdenum species to the V–Sb mixed oxide. As the amount of molybdenum increased, the amount of desorbed NH_3 increased and the desorption temperature shifted to higher temperatures. The surface of bulk molybdenum oxide (MoO_3) is acidic in nature [28] and increasing the amount of dispersed MoO_3 on a metal oxide support leads to a higher local acid concentration on the surface [29]. It is likely that the crystalline MoO_3 phase confirmed by XRD measurement causes the strong acidity on $Mo_{10}V_1Sb_{10}O_x$.

3.2. Catalytic activity for the isobutane oxidation and propane ammoxidation

Table 2 shows the results of the isobutane oxidation at 440 °C over V–Sb mixed oxides and Mo–V–Sb mixed oxides, along with those over V_2O_5, MoO_3 and α-Sb_2O_4 as references. Although isobutane conversion of 1.5% was observed without catalyst at 440 °C, this is considered negligible. The activity of α-Sb_2O_4, which is a main component of the $V_1Sb_{10}O_x$ catalyst, was quite low. Over V_2O_5, CO_x and isobutene were formed, while no oxygenated compound was produced. The V–Sb mixed oxides showed activity in ammoxidation of propane [9,11–15], where the catalytic activity strongly depended on the composition and the selectivity to acrylonitrile increased with decreasing V/Sb ratio compared to the stoichiometric one of $VSbO_4$ [11–15]. In the oxidation of isobutane over the V–Sb mixed oxide, similar phenomena were obtained, i.e., the conversion of isobutane decreased, while the selectivity of methacrolein (MAL) increased with decreasing V/Sb ratio. The main product was isobutene except CO_x on $V_1Sb_{10}O_x$ at the conversion of 7.6%. The selectivity to MAL remarkably increased by the addition of molybdenum species to $V_1Sb_{10}O_x$. $Mo_1V_1Sb_{10}O_x$ showed the highest MAL selectivity (27.6%) at the conversion of 8.1%. On the Mo–V–Sb mixed oxide with the Mo/Sb ratio >1.0, the selectivity to MAL decreased with increasing the amount of molybdenum species. On MoO_3, ethylene, isobutene and MAL were mainly formed at the conversion of 2.4%. When the volume of the reactor was minimized to prevent gas-phase radical reactions, the selectivity to MAL increased from 27.6 to 36.1% on the $Mo_1V_1Sb_{10}O_x$.

On the $Mo_1Sb_{10}O_x$ (without vanadium), the conversion of isobutane was slightly lower than that on $V_1Sb_{10}O_x$ and $Mo_1V_1Sb_{10}O_x$. The order of selectivity to MAL was $Mo_1V_1Sb_{10}O_x$ (27.1) > $Mo_2V_1Sb_{10}O_x$ (21.1) $\geqslant$ $Mo_5V_1Sb_{10}O_x$ (21.0) = $Mo_{10}V_1Sb_{10}O_x$ (21.0) > $Mo_{0.5}V_1Sb_{10}O_x$ (15.2) > $Mo_1Sb_{10}O_x$ (13.6) > $Mo_{0.1}V_1Sb_{10}O_x$ (10.9) > $V_1Sb_{10}O_x$ (9.3).

Figure 7 shows the catalytic performance of $Mo_1V_1Sb_{10}O_x$ in the oxidation of isobutane as a function of the reaction temperature. The conversion of isobutane increased with increasing reaction temperature. The selectivity to MAL slightly increased with increasing reaction temperature up to 520 °C. When the reaction was carried out at 560 °C, the selectivity to MAL drastically decreased, and propylene and methane were remarkably formed. The selectivity to CO_x decreased with increasing reaction temperature, followed by the increasing formation of other products such as isobutene and propylene. When the reaction was carried out at 520 °C in the absence of catalyst, the isobutane conversion was 39.8%, and the selectivities to propylene and to isobutene were 30.3 and 39.2%, respectively. This result indicates that the effect of gas-phase radical reaction is quite large, when the reaction is carried out above 520 °C.

The results of the propane ammoxidation at 440 °C over $V_1Sb_{10}O_x$, $Mo_1V_1Sb_{10}O_x$ and $Mo_{10}V_1Sb_{10}O_x$ catalysts are summarized in table 3. On $V_1Sb_{10}O_x$, large amount of propylene was formed, indicating that mainly oxidative de-

Table 2
Conversion and selectivity for oxidation of isobutane at 440 °C. [a]

Catalyst[b]	Conversion (%)		Selectivity[c] (%)				
	i-C_4	O_2	MAL	i-$C_4^=$	C_3H_6	Others	CO_x
$V_1Sb_{10}O_x$	7.6	100	9.3 (134.5)	25.9 (374.7)	0.0	0.9	63.9 (3699)
$Mo_{0.1}V_1Sb_{10}O_x$	7.9	100	10.9 (163.9)	28.7 (431.6)	0.0	0.0	60.4 (3634)
$Mo_{0.5}V_1Sb_{10}O_x$	7.7	100	15.2 (222.8)	17.2 (252.1)	0.0	1.3	66.3 (3889)
$Mo_1V_1Sb_{10}O_x$	8.1	99.1	27.6 (425.6)	12.5 (192.7)	0.0	0.9	59.0 (3639)
$Mo_5V_1Sb_{10}O_x$	8.7	100	21.0 (347.9)	10.8 (178.9)	0.0	0.8	67.4 (4466)
$Mo_{10}V_1Sb_{10}O_x$	7.8	100	20.1 (298.5)	12.4 (184.1)	0.0	1.6	65.9 (3914)
$Mo_1Sb_{10}O_x$	5.7	73.5	13.6 (147.5)	12.8 (138.9)	0.0	0.0	73.6 (3195)
V_2O_5	8.6	100	0.0	15.3 (250.5)	0.0	0.0	84.7 (5547)
MoO_3	2.4	37.7	9.1 (41.6)	10.8 (49.3)	0.0	19.7	60.4 (1104)
α-Sb_2O_4	0.8	12.0	0.0	69.0 (105.1)	0.0	0.0	31.0 (1888)
Empty	1.5	7.3	6.6 (18.8)	69.3 (197.9)	8.6	10.9	4.6 (52.6)
$Mo_1V_1Sb_{10}O_x$[d]	4.6	53.2	36.1 (316.1)	13.9 (121.7)	0.0	0.0	50.0 (1751)

[a] i-$C_4/O_2/N_2 = 15/5/10$ ml min^{-1}, 900 ml h^{-1} g-cat^{-1}.
[b] Atomic ratio calculated from the amount of reagents.
[c] Numbers in parentheses are the rates of formation (μmol h^{-1} g-cat^{-1}).
[d] The volume of the reactor was minimized to prevent gas-phase reactions.

Table 3
Conversion and selectivity for propane ammoxidiation at 440 °C. [a]

Catalyst[b]	Conversion (%)	Selectivity (%)			
		C_3H_6	AN	ACN	CO_x
$V_1Sb_{10}O_x$	5.2	40.4	35.6	11.8	12.2
$Mo_1V_1Sb_{10}O_x$	4.6	18.3	56.4	10.8	14.5
$Mo_{10}V_1Sb_{10}O_x$	4.6	19.2	44.2	20.1	16.5

[a] $C_3/O_2/NH_3/He = 6/12/6/16$ ml min^{-1}, 1600 ml h^{-1} g-cat^{-1} AN – acrylonitrile, ACN – acetonitrile.
[b] Atomic ratio calculated from the amount of reagents.

hydrogenation proceeded. The conversion of propane was not substantially affected, while the selectivity to acrylonitrile was enhanced by the addition of molybdenum species to $V_1Sb_{10}O_x$. On $Mo_{10}V_1Sb_{10}O_x$, the selectivity to acetonitrile was higher than on $Mo_1V_1Sb_{10}O_x$, while the selectivity to acrylonitrile was lower than on $Mo_1V_1Sb_{10}O_x$. This result indicates that C–C bond cleavage occurred on strong acid sites of crystalline MoO_3 over $Mo_{10}V_1Sb_{10}O_x$.

The oxidative dehydrogenation of isobutane to isobutene mainly proceeded over $V_1Sb_{10}O_x$ containing $VSbO_4$ and α-Sb_2O_4 phases. Under the ammoxidation conditions, this catalyst also catalyzed oxidative dehydrogenation of propane to propylene. The activity of the isobutane oxidation was quite low when vanadium species is absent, suggesting that the $VSbO_4$ phase is active for the activation of isobutane and propane. The remarkable increase in the selectivity to MAL was attained by the addition of molybdenum species to V–Sb mixed oxide. The catalytic activities of the Mo–V–Sb mixed oxide in the isobutane oxidation strongly depended on the Mo/Sb ratio. The $Mo_1V_1Sb_{10}O_x$ exhibited the highest catalytic activity. In this catalyst, we proposed the formation of highly dispersed molybdenum suboxide together with $VSbO_4$ and α-Sb_2O_4. Based on this proposed structure, the synergetic effects between molybdenum suboxide with $VSbO_4$ and/or α-Sb_2O_4 can be considered. In the oxidation of isobutene to MAL over the mechanical mixture of MoO_3 and α-Sb_2O_4, the synergetic effects between MoO_3 (and/or slightly reduced MoO_{3-x}) and α-Sb_2O_4 was reported by Delmon and co-workers [23,30–34]. This synergetic effect on the mechanical mixture cannot be explained by the formation of Mo–Sb mixed oxide. They observed the creation of a new selective (100) face of the molybdenum oxide by a partial reconstruction of the non-selective (010) face by SEM and AFM [32]. They concluded that this partial reconstruction of the non-selective (010) face to a selective (100) face caused the synergetic effect during the catalytic reaction on mechanical mixtures of MoO_3 with α-Sb_2O_4 [23,32–34]. Volta et al. also reported that the (010) face of molybdenum oxide mostly brings about total oxidation reactions, while the (100) face selectively performs partial oxidation of propylene to acrolein [35]. In the present case of $Mo_1V_1Sb_{10}O_x$, it is considered that highly dispersed molybdenum suboxide formed by the interaction between excess amount of α-Sb_2O_4 with molybdenum species. The highly dispersed molybdenum suboxide would be oriented selective (100)

face by the partial reconstruction of the non-selective (010) face, and behaves as the effective catalyst for the oxidation of isobutene to MAL. As described already, the oxidative dehydrogenation of isobutane to isobutene seems to occur on the $VSbO_4$ phase. Therefore, the improvement of the selectivity to MAL by the addition of molybdenum species to $VSbO_4$ and/or α-Sb_2O_4 can be explained by the following bifunctional mechanism. The oxidative dehydrogenation of isobutane to isobutene proceeds on the $VSbO_4$ phase, and then most part of the formed isobutene is converted to MAL on the highly dispersed molybdenum suboxide particle.

When the $Mo_{10}V_1Sb_{10}O_x$ was used for ammoxidation of propane, the selectivity to acetonitrile was higher than that on both $Mo_1V_1Sb_{10}O_x$ and $V_1Sb_{10}O_x$, indicating that the strong acidity of crystalline MoO_3 is effective for C–C bond cleavage even in the ammoxidation of propane. When large crystalline MoO_3 exists, cracking reaction (propylene, ethylene and methane formation) occurred along with non-selective total oxidation. Since it is well known that acid sites catalyzed cracking, such as C–C bond cleavage, this result can be attributed to the strong acidity of crystalline MoO_3 in $Mo_{10}V_1Sb_{10}O_x$ as observed by NH_3-TPD. The promotion effects by the addition of molybdenum ions to V–Sb mixed oxide could be also observed in the ammoxidation of propane. The bifunctional mechanism of highly dispersed molybdenum suboxides and $VSbO_4$ phase can also explain the promotion effect of molybdenum in the selectivity to acrylonitrile.

References

[1] G. Centi and F. Trifirò, CHEMTECH (April 1994) 18.
[2] H.H. Kung, Adv. Catal. 40 (1994) 1.
[3] G. Centi, Catal. Lett. 22 (1993) 53.
[4] S.T. Oyama and J.W. Hightower, *Catalytic Selective Oxidation*, ACS Symp. Ser., Vol. 523 (Am. Chem. Soc., Washington, 1993) p. 1.
[5] B.K. Hodnett, Catal. Rev. Sci. Eng. 27 (1985) 373.
[6] J.F. Brazil and L.C. Glaeser, US Patent 5 008 427 (1991);
A.T. Guttmann, R.K. Grasselli and J.F. Brazil, US Patent 4 746 641 (1988);
J.P. Bartek and A.T. Guttmann, US Patent 4 797 381 (1989);
D.D. Suresh, US Patent 4 760 159 (1988).
[7] M. Hatano and A. Kayo, US Patent 5 049 692 (1991);
T. Ushikubo, Y. Koyasu and H. Nakamura, JP 157241 (1997).
[8] Y. Moro-oka and W. Ueda, in: *Catalysis*, Vol. 11 (Roy. Soc. Chem., Cambridge, UK, 1994) p. 93.
[9] G. Centi, R.K. Grasselli and F. Trifirò, Catal. Today 13 (1992) 661.
[10] V.D. Sokolovskii, A.A. Davydov and O.Yu. Ovsiter, Catal. Rev. Sci. Eng. 37 (1995) 425.
[11] R. Nilsson, T. Lindblad, A. Andersson, C. Song and S. Hansen, Stud. Surf. Sci. Catal. 82 (1994) 293.
[12] J. Nilsson, A.R. Landa-Ca'novas, S. Hanson and A. Andersson, Stud. Surf. Sci. Catal. 110 (1997) 413.
[13] G. Centi, E. Foresti and F. Guarnieri, Stud. Surf. Sci. Catal. 82 (1994) 281.
[14] G. Centi, R.K. Grasselli, E. Patane and F. Trifirò, in: *New Development in Selective Oxidation* (Elsevier, Amsterdam, 1990) p. 515.
[15] R.K. Grasselli, G. Centi and F. Trifirò, Appl. Catal. 57 (1990) 149.
[16] R.K. Grasselli and J.D. Burrington, Adv. Catal. 30 (1981) 133.
[17] L. Abello, E. Husson, Y. Repelin and G. Lucazeau, Spectrochim. Acta 39A (1983) 641.
[18] S.T. Oyama, G.T. Went, K.B. Lewis, A.T. Bell and G.A. Somorjai, J. Phys. Chem. 93 (1989) 6786.
[19] S. Takenaka, T. Tanaka, T. Yamazaki, T. Funabiki and S. Yoshida, J. Phys. Chem. B 101 (1997) 9035.
[20] N. Das, H. Eckert, H. Hu, I.E. Wachs, J.F. Walzer and F.J. Feher, J. Phys. Chem. 97 (1993) 8240.
[21] A.N. Desikan, L. Huang and S.T. Oyama, J. Phys. Chem. 95 (1991) 10050.
[22] S.-C. Chang, M.A. Leugers and S.R. Bare, J. Phys. Chem. 96 (1992) 10358.
[23] E.M. Gaigneaux, M. Dieterie, P. Ruiz, G. Mestl and B. Delmon, J. Phys. Chem. B 102 (1998) 10542.
[24] P.A. Spavack and N.S. Mcintyre, J. Phys. Chem. 96 (1992) 9029.
[25] M. Parmentier, A. Courtois and Ch. Gleitzer, Bull. Soc. Chim. Fr. 1 (1974) 75.
[26] M. Parmentier, Ch. Gleitzer, A. Courtois, Protas, J. Acta Crystallogr. Sect. B 35 (1979) 1963.
[27] M. Parmentier, A. Courtois and R.J.D. Tilley, J. Solid State Chem. 31 (1980) 305.
[28] K. Tanabe, M. Misono, Y. Ono and H. Hattori, in: *New Solid Acids and Bases* (Kodansha, Tokyo, 1989) p. 51.
[29] H. Jeziorowski and H. Knözinger, J. Phys. Chem. 83 (1979) 1166.
[30] L.T. Weng and B. Delmon, Appl. Catal. A 81 (1992) 141.
[31] B. Zhou, E. Sham, T. Machej, P. Bertrand, P. Ruiz and B. Delmon, J. Catal. 132 (1991) 157.
[32] E.M. Gaigneaux, P. Ruiz, E.E. Wolf and B. Delmon, Appl. Surf. Sci. 121/122 (1997) 552.
[33] E.M. Gaigneaux, P. Ruiz, E.E. Wolf and B. Delmon, Catal. Today 32 (1996) 37.
[34] E.M. Gaigneaux, P.E. Tsiakaras, D. Herla, L. Ghenne, P. Ruiz and B. Delmon, Catal. Today 33 (1997) 151.
[35] J.C. Volta, O. Bertrand and N. Floquet, J. Chem. Soc. Chem. Commun. (1985) 1283.